DESIGN OF SMART STRUCTURES FOR WIND TURBINE BLADES

Supeni E.E.[1], Epaarachchi J.A.[2], Islam M.M.[2] and Lau K.T.[2,3]

[1]Department of Mechanical Engineering,Faculty of Engineering
Universiti Putra Malaysia,Malaysia
[2]Centre of Excellence in Engineered Fibre Composites
University of Southern Queensland, Australia
[3]Department of Mechanical Engineering
Hong Kong Polytechnic University HongKong, China
E-mail:ErisElianddy.Supeni@usq.edu.au

ABSTRACT

The wind turbine blade is a very important part of the rotor. Extraction of energy from wind depends on the design of the blade.The advancement of fibre composite materials have provided the best solutions to overcome inefficiencies caused by traditional materials used in wind turbine construction. At present, the majority of wind turbine blades are constructed with glass fibre reinforced plastic (GFRP). The use of composite materials eventually have solved some of the problems associated with efficient operation of horizontal axis wind turbines (HAWTs) such as gravitational forces due to weight but there are other unresolved problems such as long term material property degradation, local shape deformation of the profile of the wind turbine blades etc. This project aims to address the adverse structural response of the blade profile with the variation of operational parameters such as wind velocity and material properties on blade's performances. For this reason, the shape memory alloy (SMA), which is Nitinol (NiTi) has been embedded in the blade to alleviate the load. A parametric blade model utilising the Abaqus finite element program has been developed to efficiently predict the deflection of the blade. Result obtained from Abaqus is compared with the current experimental work. It was found that the numerical model developed in FEA agreed relatively well with the experimental work, thus validating underlying assumptions.

Keywords**:** GFRP**,** SMA, FEA,NiTi

INTRODUCTION

The utilization of wind energy is not a new technology but has caught attention due to the rediscovery of a conventional wind power technology. It has been proven in the past as that it was used to capture the wind as much as possible in order to generate power(Erich, 2009). In 2007, the government has committed to ensure that 20 per cent of Australia's electricity supply would come from renewable energy sources by 2020 by establishing the expanded national Renewable Energy Target (RET) scheme. The enhanced RET scheme commenced on 1 January 2010 and is projected to deliver more than 45,000 gigawatt hours of electricity in 2020. It is expected to unlock more than $AUS20 billion in investment over the next decade (ACEC, 2012).

Rapid development in material technology has given influential impact on some variation structure of the wind turbine. The variation mainly depends on positive reaction for lowering the prices of wind turbine construction and operational cost. As known, there are a lot of materials such as composite materials to be used in wind turbine structures such as for tower, blade hub and nacelle. The focal point in the system where the wind is converted into useable energy is the wind turbine blade. Around more than 10,000 blades have been supplied over 10 years to the strictest quality standards which near to aerospace quality at industrial cost. The blades have been customized designed which tailored to customer's turbine specification (Nolet, 2011). The blade, as part of the prime mechanical wind turbine rotor, is a key element within the wind turbine system and as such research aimed at improving blade performance is of great importance(Glauert, 1983). It is definitely an influential component for system efficiency. In the evolution era, dimensions and number of component vary on the basis of turbine strength. Its development in the past varied from canvas to wood and sheet metal. But, in recent modern era, composite has been implemented by all turbine manufacturer (Eker et al., 2006). The anatomy of the modern wind turbine is illustrated in Figure 1.

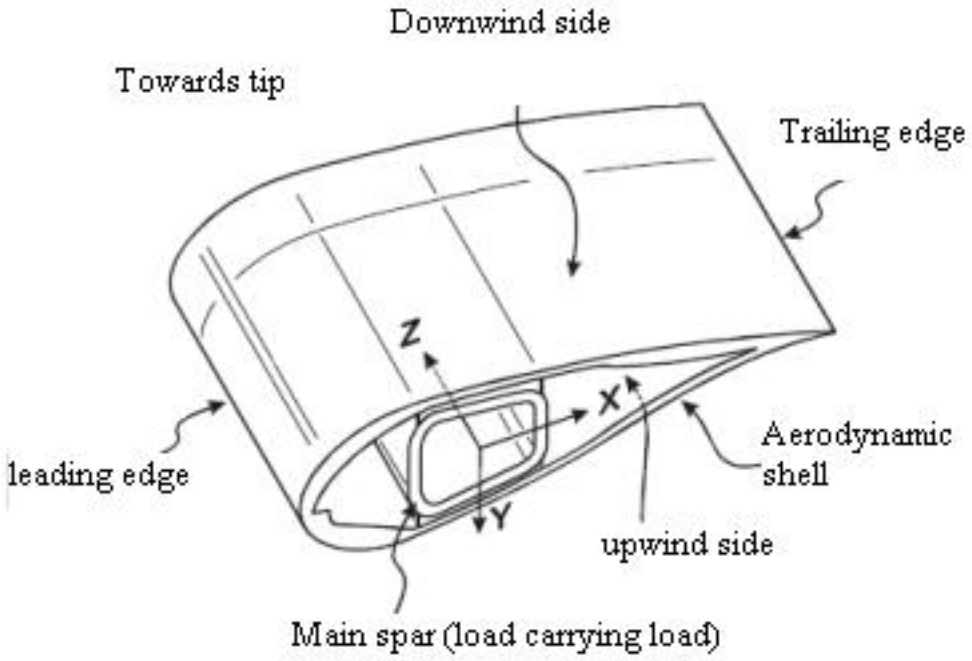

Figure 1. Typical cross sections of wind turbine blade (Sorensen et al., 2004)

Wind turbine blades are required to preserve an optimum cross section for aerodynamic efficiency by optimizing the lift to generate the maximum torque to drive the generators. Figure 2 shows aerodynamic mechanism of the wind blade when there is wind flow. However, several factors such as static and dynamic loading, fatigue resistance, rigidity, weight, sound emission and appearance have adverse impact on a wind turbine (Epaarachchi and Clausen, 2006), (Spera, 2009), (Wood, 1991).

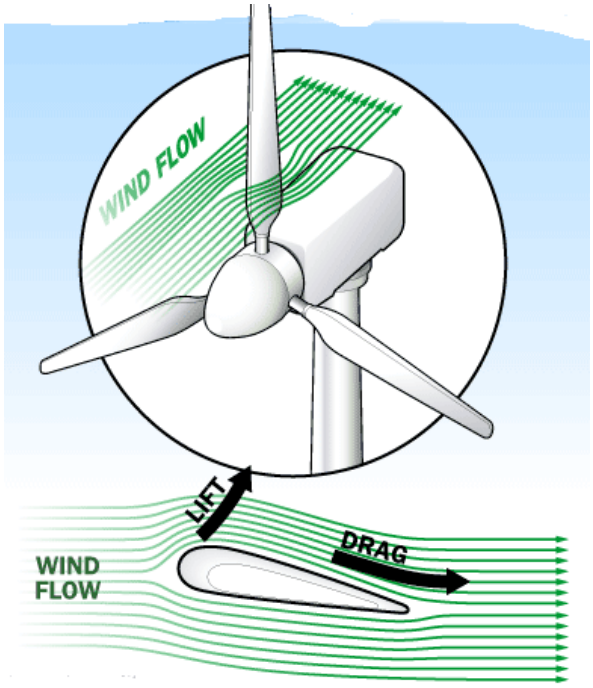

Figure 2. Aerodynamic of the wind turbine blade (Eggleston and Stoddard, 1987)

BLADE LOADING

Aerodynamic Forces

An aerodynamic force is complicated in nature and hard to investigate. These forces can be unsteady and vary in a non-linear way along the axis of blade, also made complex by the random condition of the atmosphere. In studying them, stochastic or statistical testing must be relied on rather than more direct deterministic testing like through wind tunnel testing. The aerodynamic forces acting on a blade at steady state are shown in Figure 3. Due to the aerodynamic pressure acting on the blade's surface, the resultant lift force L_A acts perpendicular to the resultant wind velocity, W_A and also the drag force D_A, act parallel to the resultant wind velocity.

The resultant velocity $W_A = \sqrt{(r\Omega + W_A)^2 + U_0^2}$ (1)

$$= U_0\sqrt{(\lambda + \frac{W_A}{U_0})^2 + 1} \quad (2)$$

The aerodynamic forces on the blade section simply can be expressed as

$$L_A = \frac{1}{2}\rho C_P W_A^2 \Delta A \quad (3)$$

or

$$L_A = \frac{1}{2}\rho C_P U_0^2 [(\lambda + \frac{W_A}{U_0})^2 + 1]\Delta A \quad (4)$$

where $\lambda = \frac{\Omega r}{U_0}$, tip speed ratio, with Ω is the rotational speed of the turbine, r is the radius of the blade section considered, ρ is the density of the air and ΔA is the considered small area of a wind turbine blade. As a consequence, aerodynamic force on the blade at wind velocity V can be easily determined by multiplying aerodynamic forces at wind velocity U by factor of $\frac{V^2}{U^2}$, as long as C_P is constant. (Note:W_A is considerably smaller than $r\Omega$).

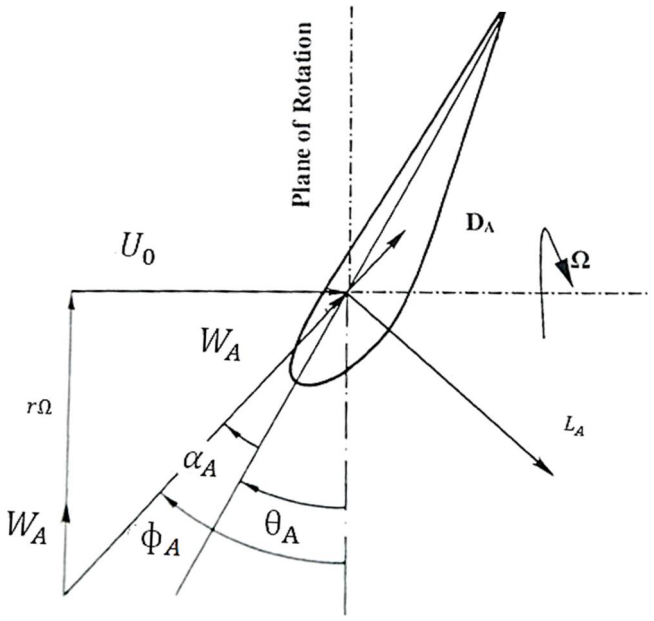

Figure 3. View of aerofoil section at the radius r along the blade, relative to the hub blade(Eggleston and Stoddard, 1987)

Analysis of aerodynamic pressure along the blade is a complex task. Wood (1991) used a panel code to overcome some of the deficiencies found in the blade element theory (BET). In the panel code, a blade is divided into 40 strips along the blade axis and 10 pressure centers along the chord. Wood has shown that by using full – three dimensional analysis, the blade surface pressure in steady wind can be estimated more accurately than with BET. The panel code determines the normal pressures acting on the blade surface and so estimates the drag forces, D_A. As such the predicted performance of wind turbine blade will be overestimated.

Inertial, Gravity and Structural Forces Blade Design and Structural Analysis

These forces arise as a result the blade mass, blade rotation and gravity and contribute to the total forces acting on a wind turbine. A combination of aerodynamic, gravitational and inertial forces lead to two significant blade motion whilst rotating: blade flapping and blade lead-lag as illustrated in Figure 4. Blade flapping, motion of the blade out of its plane rotation, is fundamentally caused by variation in wind flow. Blade lead-lag is essentially caused by the operating blade rotating, in gravitational field. The centrifugal force acting on the blade creates a counter acting moment to that induced by the

aerodynamic pressure. As such, centrifugal force reduces the deflection, *d* on aerodynamically loaded blade.

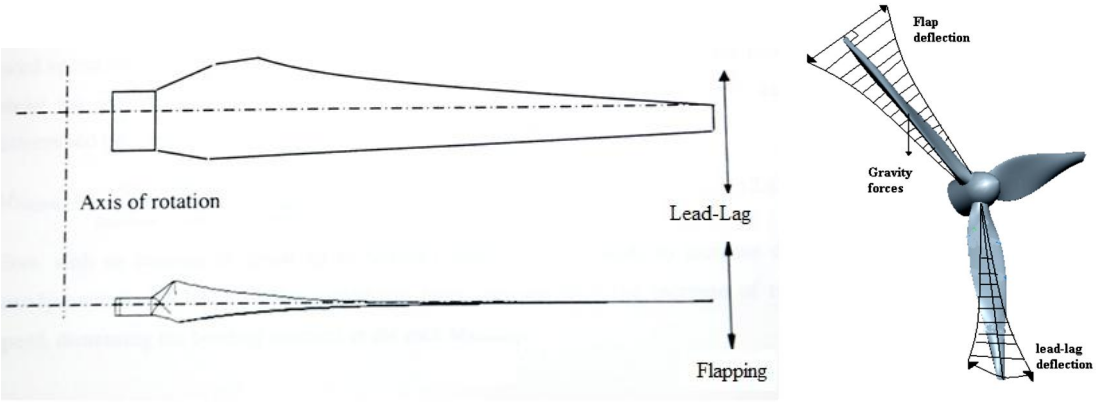

Figure 4. Lead-lag and flapping moment (schematic view)

Figure 5 shows the blade motion, let the resultant aerodynamic force be δF acting on a blade surface of δA at radius in the direction *Y*(Note: gravity forces and in-plane component of the aerodynamic pressure are perpendicular to the flapping plane) on a blade in steady operation at rotational speed Ω (< rated operational speed). At this particular instant the total bending moment at the root end about the axis perpendicular the blade's rotational axis (Flapping moment) can be determined by:

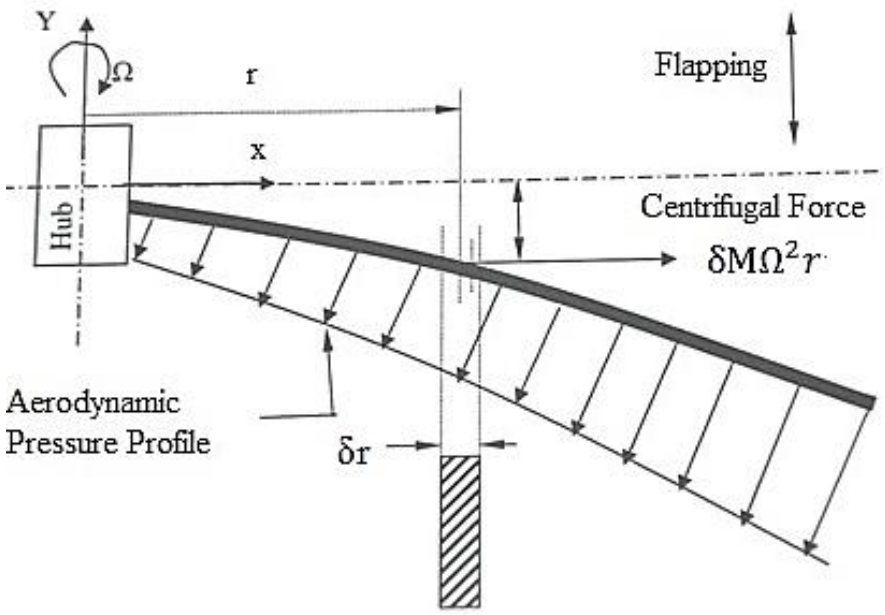

Figure 5. Inertial forces acting on a wind turbine blade before steady operation at constant speed of Ω (schematic view)

$$M_{Flapping} = \sum_{Blade\ length}(\sum_{chord} \delta Fr - \sum_{chord} \delta M\Omega^2 rd) \quad (5)$$

Here, with an increase in speed up to turbine's rated speed, *d* deflection tends to increase due to aerodynamic pressure load. However, the centrifugal force increase with

the increase of turbine speed, decrease the bending moment at the root $M_{Flapping}$ (Epaarachchi, 2002).

NACA 4-Digit Airfoil Selection

The development of efficient (low-drag) airfoils was the subject of deep experimental investigations in the 1930s. These airfoils were standardized by the National Advisory Committee for Aeronautics (NACA), and extensive lists of data on lift coefficients were reported(Manwell et al., 2009). The comparative study has been taken in order to develop NACA 4412 blade profile. Figure 6 shows variation of the optimum power coefficient with the design tip-speed ratio for a blade made of NACA 4-digit airfoil families. It is seen that C_p increases rapidly with TSR up to its optimum value after which it decreases gradually with a slower rate. The optimum range of the TSR is observed to lie between 6 and 11, depending on the type of airfoil. The effect of wind shear and tower shadow resulted in a reduction of the power coefficient by about 16%. The value of the design TSR at which $C_p$max occurs is also reduced by about 9%. It is also observed that blades with NACA 4412 produces higher power output as compared with other airfoil types.

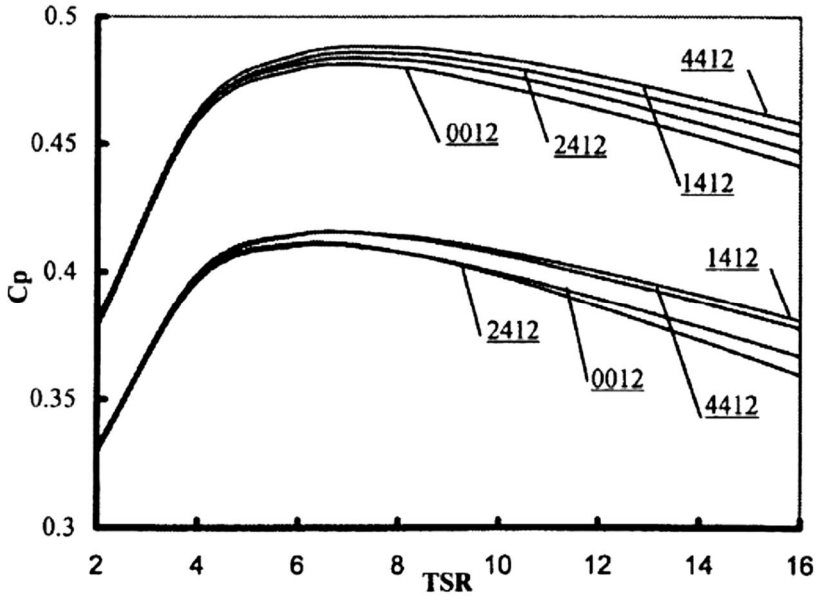

Figure 6. Variation of the optimum power coefficient with TSR for a three bladed rotor of NACA 4-digit airfoil(Malawi, 2010)

Smart Structures Application

Shape memory alloys (SMAs) have been defined by several researchers as smart material with all the various definitions pointing to the unique properties associated with SMAs. SMA as a metal alloy can memorize and revert to a specific shape after considerable deformation. Patoor et al. (2006) defined SMAs as metallic alloys that can undergo martensitic phase transformations as a result of applied thermo-mechanical loads and are capable of recovering permanent strains when heated above a certain transformation temperature(Patoor et al., 2006). SMAs are defined by their remarkable ability to sustain and then recover large super elastic strains by stress and temperature

dependent crystallographic transformations (Srinivasan and McFarland, 2001) (Armstrong and Lilholt, 2000). SMAs possess sensing and actuating functions and have the potential to control the mechanical properties and responses of their hosts due to their inherent unique characteristics of SME and super elastic. When integrated into structural components, SMAs perform sensing, diagnosing, actuating and repair or healing functions, thereby enhancing improved performance characteristics of their hosts (Zhang et al., 2007)(Lau et al., 2002a). In the literature, SMA actuators have been proposed for use in many engineering structures. Many studies have suggested SMA wires can be embedded in a composite(Lagoudas and Bo, 1994)(Zhou and Lloyd, 2009). The embedding approaches have been investigated by Yongsheng et al. who studied the behavior of SMA strips that have been thermally trained to memorize a bent shape, pre-strained to a circumferential shape(Yongsheng et al., 2009)(Lau et al., 2002b).

On heating, the strips tend to recover the memorized shape and the plate is forced to bend. As in-plane displacements of the strips relative to the plate are allowed in this design, de-bonding and rapid ageing are prevented during multi-cycle actuation. Rizzoni et al. studied the actuation characteristics of NiTistrips/ribbon working in bending and fixed to the surface of a polymeric plate. The preliminary experimental assessment of the heat treatment parameters that are needed to memorize a bent shape has been presented. Typical application of such composite is the control of the geometry of blades to increase the performance of cooling fans in earth-moving engines (Rizzoni et al., 2011). Nowadays, fibre reinforced composites have already gained large interest and increased application in diverse fields. This is mainly due to their inherent high stiffness-to-weight ratio, corrosion resistance and controlled anisotropic properties. Shape memory alloys (SMA) are commercially used in a variety of actuator, clamping and fixing devices (Zhou and Lloyd, 2009).

Smart Wind Blade Concept

The series investigations of the graded sandwich panel will be tested based on the cantilever beam are focused on implementation and testing of the embedded SMA under static loading. Parameters such as time response for actuation, temperature surface, current applied will be measured during the test.FEA will be used to simulate the deflection and optimize the experimental work analysis.

Modeling Process and FEA

Before plotting in 3D, predefined coordinates have been precisely generated in the Matlab and all the respective points have been imported into the coordinate system (CSYS) in Pro E(USQ, 2009). After activating the coordinate system, cross sectional area of chord has been generated using surface blending and swept protrusion. For simulation of static loading, a design blade was plotted in Pro E which is shown in Figure 7. The specification of the profile is illustrated in Table 1. Then, the three parts were properly assembled into the blade assembly and saved into Initial Graphics Exchange Specification (IGES) format. In Abaqus 6.11, the drawing will be imported to test the static loading as shown in Figure 8(Abaqus, 2011)(Yushu and Chuanguo, 2010).

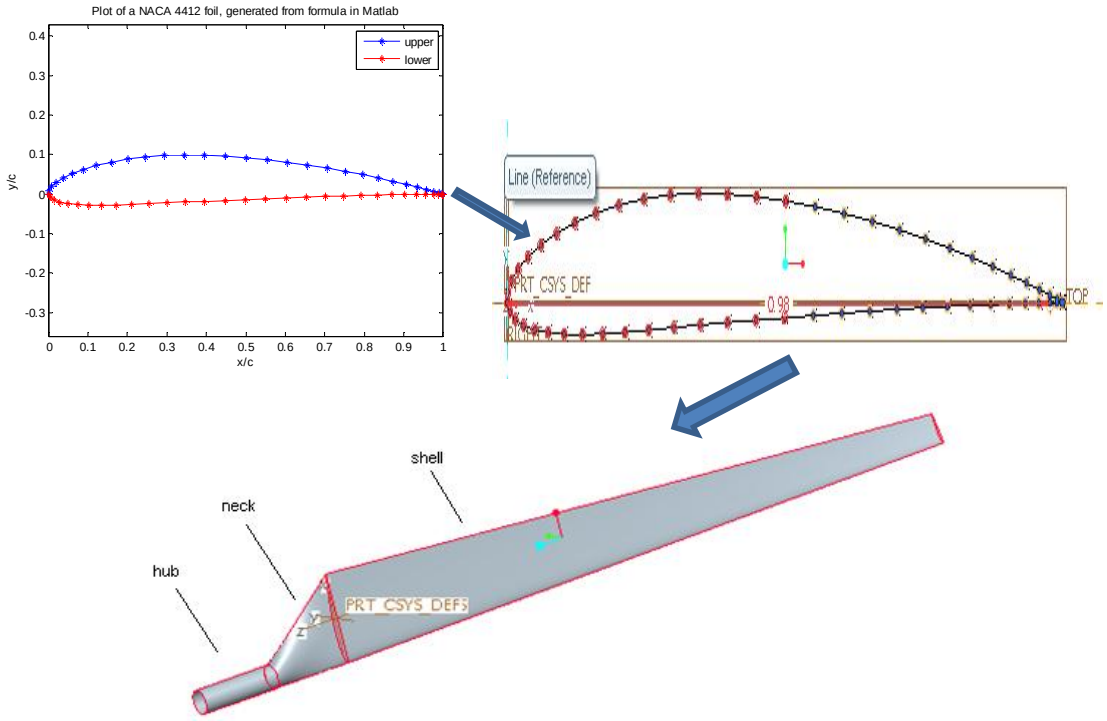

Figure 7. The coordinate points for NACA 4412 into Pro E for blending surface

Table 1. Geometric details of NACA 4412 (Selwin et al., 2008)

Particular of blade geometry	
power	5kW
root chord length	330 mm
tip chord length	130 mm
blade length	2500 mm
hub diameter	67.5 mm
hub blade to neck length	300 mm
twist from the root to tip	18°

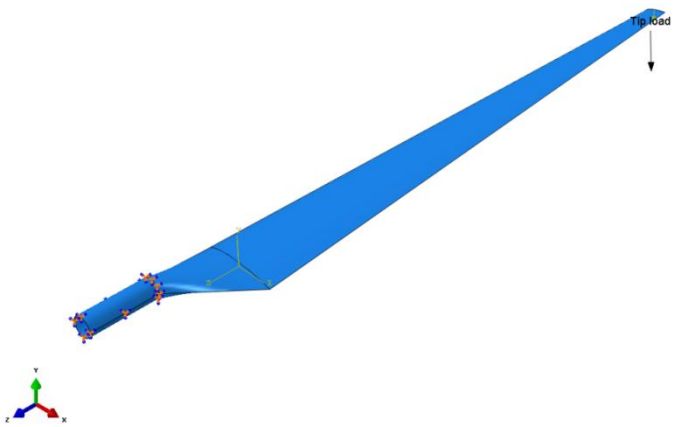

Figure 8. Boundary condition, load applied at the tip and meshing process

Figure 9 illustrates the displacement along the blade. At the free end there are no boundary conditions and therefore the displacement is much larger at the tip and displacement is constrained at the hub as there is restriction point. Figure 10 shows the strain pattern concentration simulated using Abaqus. Higher strain values are predicted at the root rather than at the tip section. This was also proven by Grujicic et al. (2010) where simulation was carried out using Ansys. Figure 11 depicts the fabrication of the ply configuration has been simulated at $[0^0/90^0/-45^0/+45^0]$**.** Similarly**,** higher contribution of the stress at the root rather than at the tip is observed.

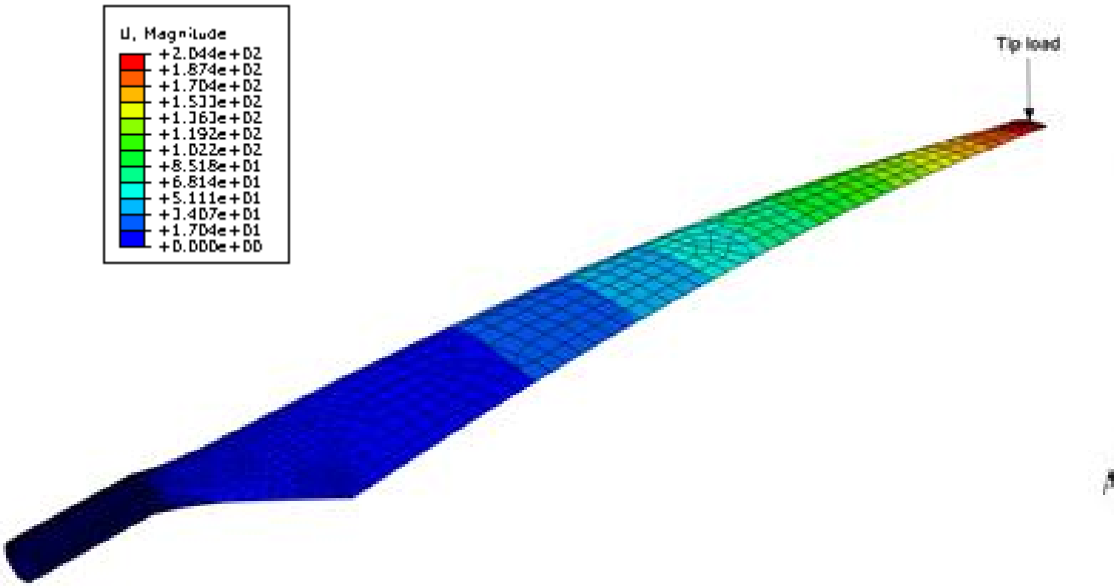

Figure 9. Displacement profile along the blade at isoview angle

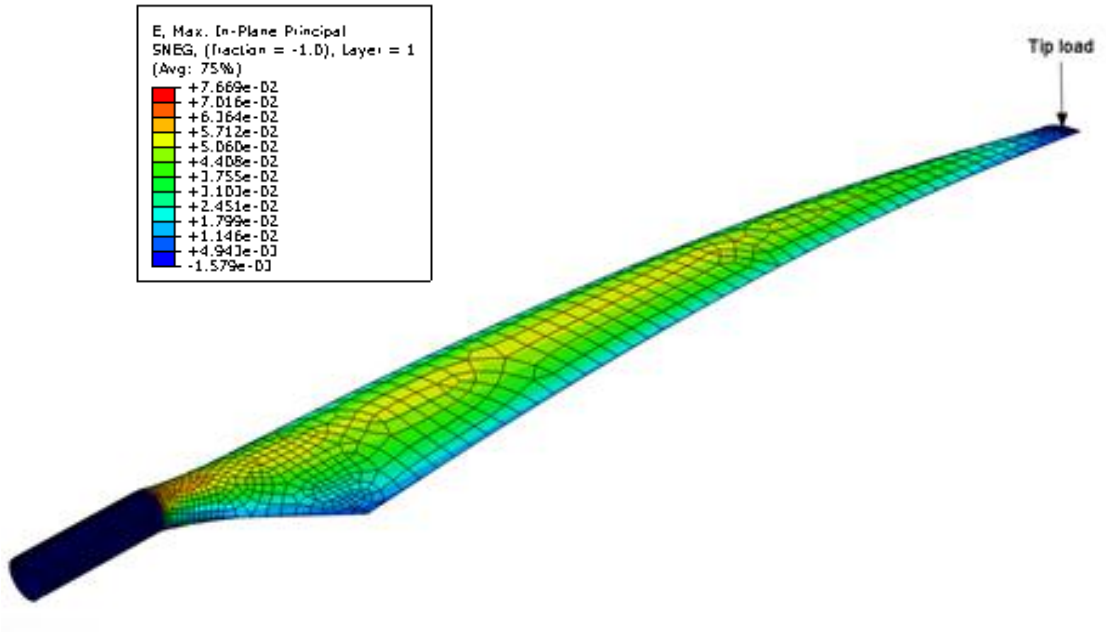

Figure 10. Strain pattern at isoview angle

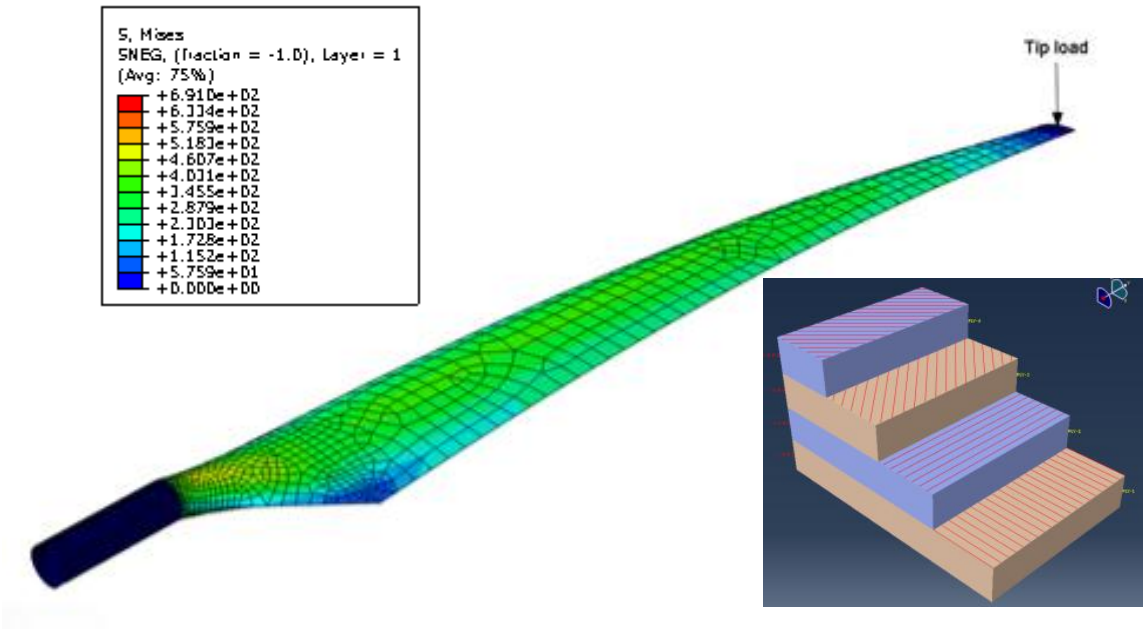

Figure 11. Stress pattern at isoview angle

NUMERICAL MODEL

A numerical model has been developed to analyse the deflection behavior of the graded GFRP (glass fibre reinforced plastic) beam, using Abaqus/Explicit 6.11code. The graded beam with the element type SC8R was modeled geometrically using the mechanical properties (Table 2) for the static loading as shown in Figure 12. Then the numerical modeling has been experimentally validated based on the cantilever beam as shown in Figure 13.

Table 2. Mechanical properties of GFRP

Glass Fibre Epoxy	**E-glass UD Kinetix R246TX**
E_1 (MPa)	34412
E_2 (MPa)	6531
V_{12} (MPa)	0.217
G_{12} (MPa)	2433
G_{13} (MPa)	1698
G_{23} (MPa)	2433
$\rho(kg/m^3)$	2000

In order to validate the result given by Abaqus, comparison on the tip deflection is made with Strand 7. Table 3 shows the comparison made on the tip deflection between Abaqusand Strand 7 deflection at the tip are 40.174mm and 41.271 mm respectively.About 2 % of percentage difference was discovered. However, in Figure 13 Abaqus was able to simulate nonlinear contour pattern variation particularly at the tip where the concentrated load is applied.

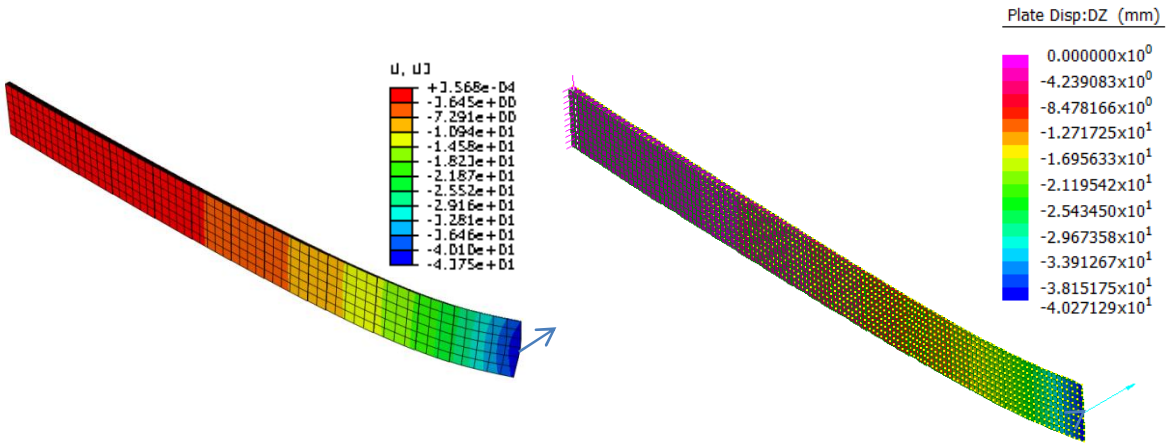

Figure 12. Deflection pattern using Abaqus (left) and Strand 7 (right)

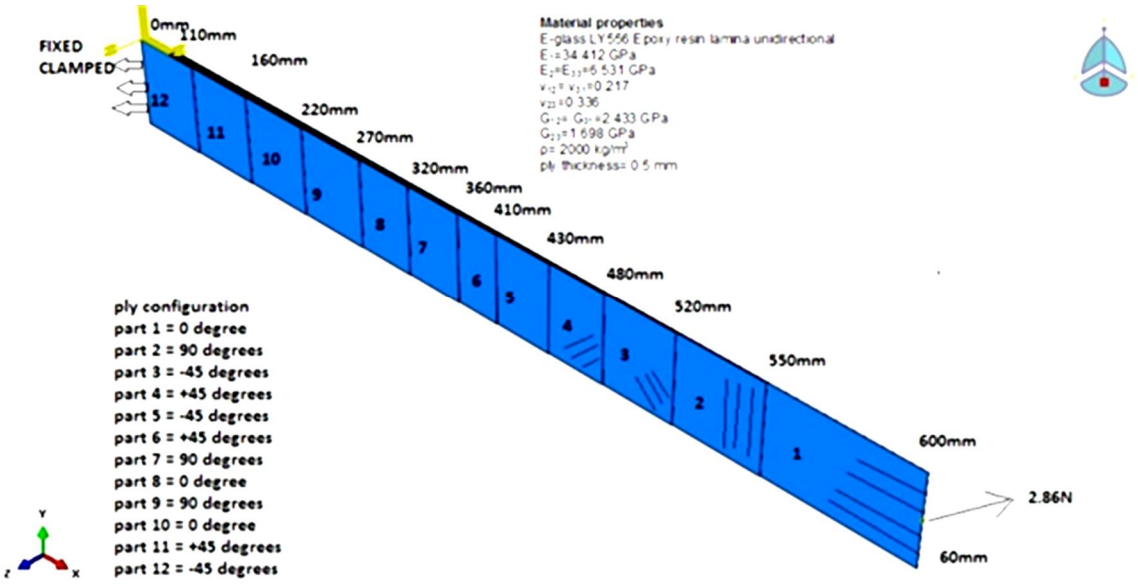

Figure 13. Graded GFRP beam model layout diagram

Table 3. Comparison of FEA

Simulation	Abaqus	Strand 7
Tip deflection (mm)	40.174	41.271

EXPERIMENTAL DESIGN

Specimens for Smart Structure Testing

The graded GFRP beam was fabricated in the CEEFC laboratory. Five samples have been experimentally tested in the cantilever beam and designated test rig has been used for deflection test as shown in Figure 14. The graded thin shell was fabricated using hand lay-up that consisted of a unidirectional E-glass fiber/epoxy composite laminated with the configuration lay-up of $[0^0/90^0/-45^0/+45^0/-45^0/+45^0/90^0/0^0/90^0/0^0/+45^0/-45^0]$ respectively with the lamina elastic material properties. In order to reduce shear load

bearing strength, the inner foam such as expanded polystyrene (EPS) has been tied constraint to GFRP laminate. Before experimental work is carried out the simulation was madeto predict the deflection of the panel. Figure 15 shows the model used in simulation is in agreement with the experimental work. Reasonable agreement was achieved between both methods. The current findings shows that by using EPS the blade deflection could be minimized by about 35 % in experimental whilst 39 % in FEA. To develop the SMA wire displacement, a test on the relationship of deformation with load applied with hot and cold wire has been experimentally carried out. The DC power supply model GW Instek GPC 1850D has been used to drive the current flow in SMA wire.

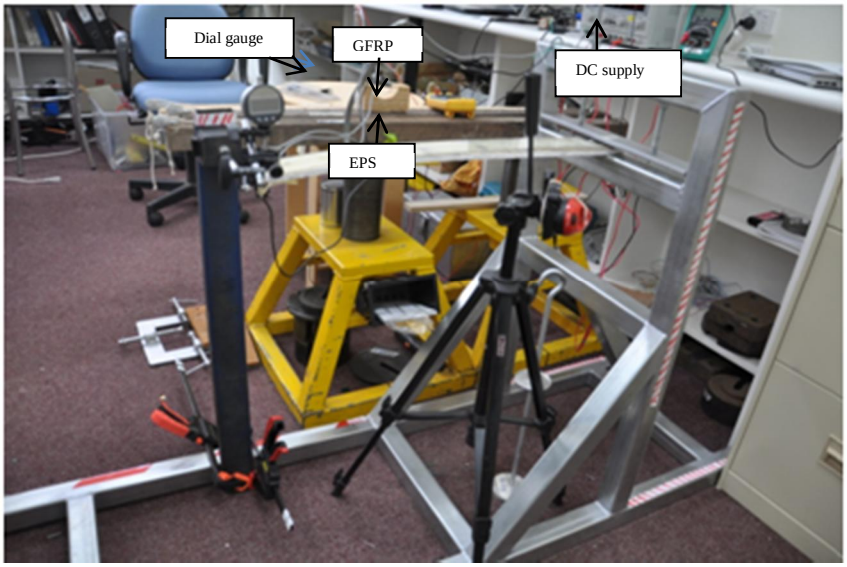

Figure 14. Experimental test rig

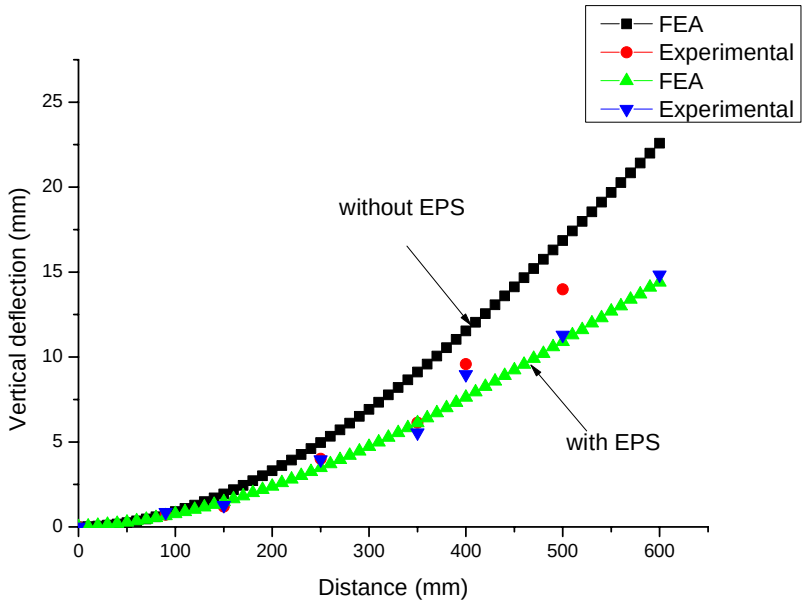

Figure 15. Comparison of vertical deflection between FEA and Experiment (with EPS/without EPS)

Figure 16 presents the experimental setup for the load test. The FlexinolSMA wire with diameter of 0.51 mm has been used for this purpose. It is expected that the deflection will be reduced as well as the SMA wire is embedded in the composite blade. At the early stage, load test has been carried out with the voltage supplied from the constant DC power supply unit at 5.50 V with current 2.2. Assuming the pulley is light, the rotational inertia is negligible. Moreover, no force is required to turn the frictionless pulley, so it can be assumed that the bearing of pulley is frictionless. Figure 17 shows the comparison of the load test wire with and without current being applied. It was estimated 2 mm of pulling force existed at different loads.

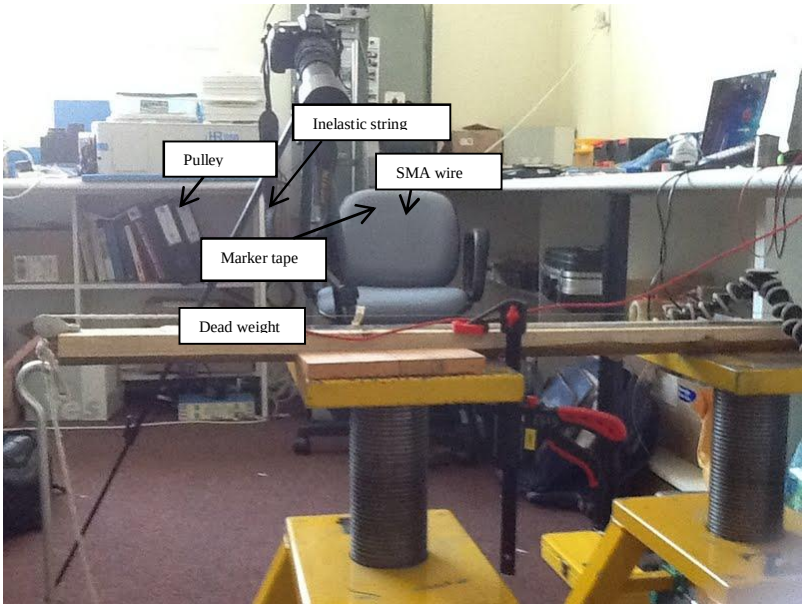

Figure 16. Experimental setup for the load test

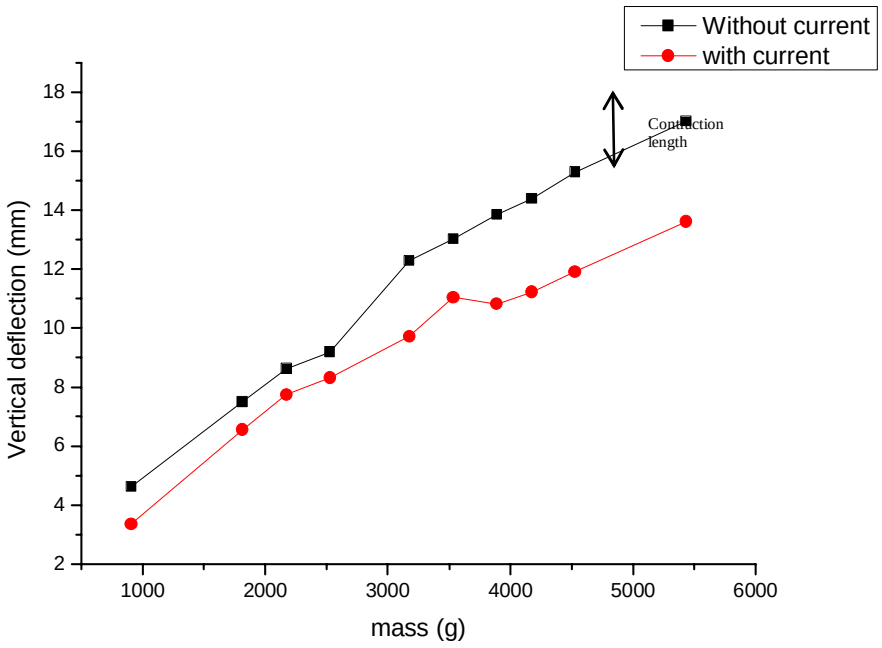

Figure 17. Load test of SMA wire

Table 4 shows the result of the pulling force of the SMA when current is applied. It has been observed in this test, the relationship of the current is proportional to the heat generated in the wire as well. Figure 18 shows the temperature relationship with the voltage applied. Temperature parameter is used to monitor the transformation and temperature lies in the range martensitic region. To determine the transformation temperature of the SMA, the DSC (direct scanning calorimeter) has been used as depicted in Figure 19. In this test, the critical deformation and shape recovery are explained according to the lattice parameters changes through a phase transformation between austenite and martensite and the characteristics of the crystal structure.

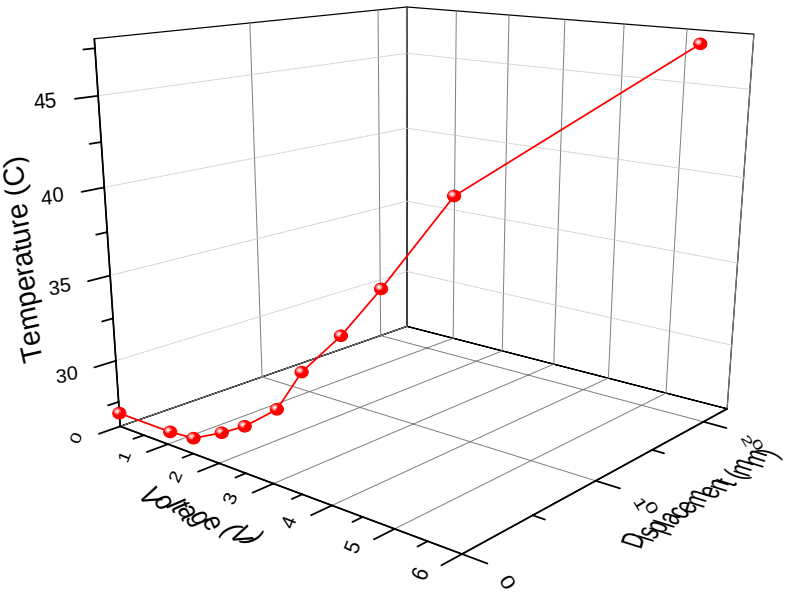

Figure 18. Relationship between the voltage, surface temperature and displacement

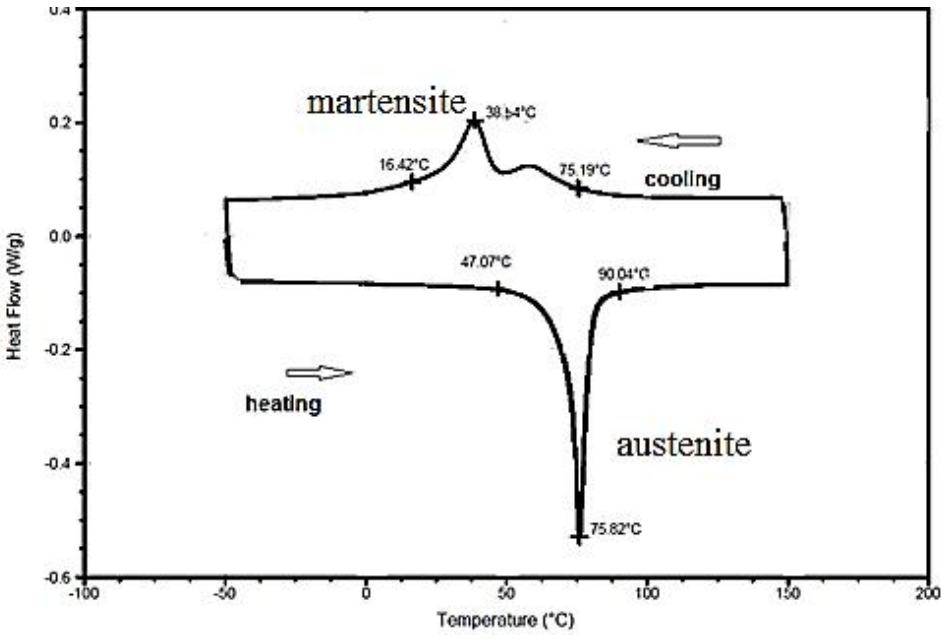

Figure 19. Transformation temperature of the SMA

Table 4. Pulling test load of 907g

Voltage (V)	Initial displacement (mm)	Final displacement (mm)	Distance change (mm)
1	15.99	15.99	0.00
2	15.99	15.90	0.09
3	15.99	15.53	0.46
4	15.99	14.36	1.63

Problem Encountered During Experiment

The NiTi will be embedded between the EPS and the FGRP composite panel which is parallel to neutral axis. The fabrication of the panel is illustrated in the Figure 20. Currently, the fabrication of SMA embedded on the sandwich panel has been ongoing. However, there is difficulty particularly in embedding the pre strain wire although the clamping device has been used. The turn buckle is used to pull the wire up to 4 percent pre-strain. In this arrangement, the NiTi embedded in fibres are free to move during the phase transformation process and also must resist degrading and destructing the graded composite blade when the actuation process takes place.

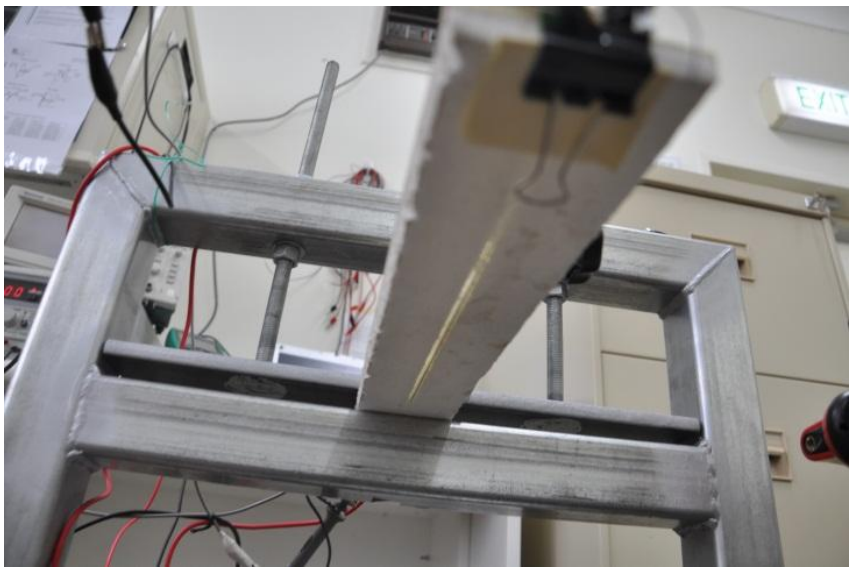

Figure 20. SMA fabrication with the burn EPS

CONCLUSION

The investigation of the deflection of the graded GFRP laminated with adhesively epoxy resin under concentrated loading is presented. Current findings and results of the numerical simulation and its correlation with experimental results have been discussed. Finite element analysis using Abaqus is able to predict satisfactorily deflection compared with the experimental works. Future works and problem encountered are also discussed. The SMA which is embedded in composite is expected to alleviate the deflection.

ACKNOWLEDGEMENT

The authors would like to thank the UPM and MOHE of Malaysia for providing the research facilities and support in CEEFC of University of Southern Queensland, Australia.

REFERENCES

Abaqus 2011. *Release Note 6.11*.

Acec 2012. There's Power In Wind: Fact Sheet. *In:* Council, A. C. E. (Ed.).

Armstrong, W.D. & Lilholt, H. 2000. The time dependant, super-viscoelastic behaviour of niti shape memory alloy fiber reinforced polymer matrix composites. *Materials Science and Engineering,* B68**,** 149-155.

Eggleston, D.M. & Stoddard, F.S. 1987. *Wind turbine engineering design*.

Eker, B., Ovan, A. & Vardar, A. 2006. Using of composite material in wind turbine blades. *Journal of Applied Sciences,* 6**,** 2917-2921.

Epaarachchi, J.A. 2002. *The development and testing of a new fatigue life procedure for small composite wind turbine blades incoporating new empirical fatigue life prediction and damage accumulation models for glass fibre reinforced plastics.* Phd Thesis, The University Of Newcastle.

Epaarachchi, J.A. & Clausen, P.D. 2006. The development of a fatigue loading spectrum for small wind turbine blades. *Journal of Wind Engineering and Industrial Aerodynamics,* 94**,** 207-223.

Erich, H. 2009. Wind turbines: fundamentals, technologies, application,The Facts : A guide to the technology, economics and future of wind power. *In:* London; Sterling, V., Earthscan. (Ed.) *European Wind Energy Association.*

Glauert, H. 1983. *The elements of airfoil and airscrew theory.*

Grujicic, M., Arakere, G., Sunbramaniam, E., Sellapan, V., Vallejo, A. & Oze, M. 2010. Structural responce analysis, fatigue-life prediction, and material selection for 1 Mw hawt wind blade turbine. *Journal of Material Engineering And Performance***,** 790-801.

Lagoudas, D.C. & Bo, Z. 1994. The cylindrical bending of composite plates with piezoelectric and sma layers. *Smart Materials and Structures,* 3**,** 309–317.

Lau, K.T., Chan, A.W.L., Shi, S.Q. & Zhou, L.M. 2002a. Debond induced by strain recovery of an embedded niti wire at a niti/epoxy interface: Micro-scale observation. *Materials Design,* 23**,** 265-270.

Lau, K.T., Tam, W.Y., Meng, X.L. & Zhou, L.M. 2002b. Morphological Study on twisted niti wires for smart composite systems. *Materials Letters,* 57**,** 364-368.

Malawi, K. 2010. Special issues on design optimization of wind turbine structures. *In:* Al-Bahadly.2, I. (Ed.) *Wind Turbines. Intech. I.*

Manwell, J.F., Mcgowan, J.G. & Rogers, A.L. 2009. *Wind energy explained : Theory, Design And Application,* Chichester, UK.

Nolet, S.C. 2011. Composite wind blade engineering and manufacturing. *In:* Tpi Composites, I. (Ed.).

Patoor, E., Lagoudas, D.C., Entchev, P.B., Brinson, L.C. & Gao, X. 2006. Shape memory alloys, Part I: General properties and modelling single crystals. *Mechanics of Materials,* 38**,** 391-429.

Rizzoni, R., Merlin, M. & Daniele, C. 2011. Bending properties of heat-treated niti strips for actuation of smart reinforced beams. pp.1-7.

Selwin, R.J., Christopher, T., Thanigairasu, G. & Rao, B.N. 2008. Finite elemnt analysis with an improved failure criterion for composite wind turbine blade. *Forsch Ingenieurwes***,** pp. 193-197.

Sorensen, B.F., Jørgensen, E., Christian, P.D. & Jensen, F.M. 2004. Improved design of large wind turbineblade of fibre composites based onstudies of scale effects (Phase 1). *Risø-R-1390(En) (Ed.). Denmark.*

Spera, D.A. 2009. *Wind turbine technology*: *Fundamental Concepts of Wind Turbine Engineering,* New York.

Srinivasan, A.V. & Mcfarland, D.M. 2001. *Smart Structures-Analysis and Design* United Kingdom.

Usq 2009. *Pro Engineers Note Module.*

Wood, D.H. 1991. A Three-dimensional analysis of stall delay on hawt. *Journal of Wind Engineering and Industrial Aerodynamics,* 37**,** 1-14.

Yongsheng, R., Yang, S. & Wang, X. 2009. Structural modeling of sma fiber hybrid active thin-walled composite beams. *Composite Structures,* 91**,** 120-130.

Yushu, W. & Chuanguo, F. 2010. *Analysis of Structural Engineering and Examples Explanation In Detail Of Abaqus,* Beijing.

Zhang, R.X., Ni, Q.Q., Natsuki, T. & Iwamoto, M. 2007. Mechanical properties of composites filled with sma particles and short fibres. *Composite Structures,* 79**,** 90-96.

Zhou, G. & Lloyd, P. 2009. Design, manufacture and evaluation of bending behavior of composite beams. *Composites Science and Technology,* 69**,** 2034–2041.

LIST OF ABBREVIATION

GFRP : Glass fibre reinforced plastic
SMA : Shape memory alloy
FEA : Finite element analysis
NiTi : Nitinol
CEEFC: Centre of Excellence in Engineered Fibre Composites
UPM : Universiti Putra Malaysia
MOHE: Ministry of Higher Education
NACA : National Advisory Committee for Aeronautics
TSR : Tip speed ratio
C_p : Coefficient of power
EPS : Expanded polystyrene